Journal of Materials Chemistry A

PAPER

View Article Online
View Journal | View Issue

Cite this: J. Mater. Chem. A, 2017, 5, 15260

Hierarchically ordered arrays with platinum coated PANI nanowires for highly efficient fuel cell electrodes†

Ruili Sun,[ab] Zhangxun Xia,[a] Lei Shang,[ab] Xudong Fu,[a] Huanqiao Li,[a] Suli Wang*[a] and Gongquan Sun *[a]

Received 22nd March 2017
Accepted 24th May 2017

DOI: 10.1039/c7ta02500a

rsc.li/materials-a

The fabrication of a novel electrode architecture with multi-scale orderliness is an effective strategy to enhance Pt utilization and decrease the mass transport polarization loss of proton exchange membrane fuel cells (PEMFCs). Here we report a hierarchically well-defined electrode with Pt nanowhiskers on aligned nanowires by a magnetron sputtering method. With the crystallographically preferential growth of Pt (111) facets, in association with the electron modification effects of PANI on Pt nanowhiskers, the electrode achieves outstanding electrochemical activity towards the oxygen reduction reaction (ORR) with a 2.19-fold enhancement of the specific activity and a similar mass specific activity at 0.9 V (*vs.* the RHE), compared to the state-of-the-art Pt–C electrode. The PEMFC fabricated with the Pt–PANI-GDL electrode shows excellent performance with a peak power density of 542 mW cm^{-2}, and a cathode mass specific power density of 5.7 W mg_{Pt}^{-1}, which is 39% greater than that of PEMFCs equipped with a Pt–C electrode for enhanced electrochemical activity and mass transport.

Introduction

Polymer electrolyte membrane fuel cells (PEMFCs), as a class of the most promising alternative sources of energy technologies, have drawn much attention because of their high power density, quick start-up and low pollutant emission.[1–3] However, the massive use of the scarce platinum group metals (PGMs) is still one of the major challenges for the large scale commercialization of PEMFCs.[4–7] Despite the great efforts that have been made to substitute PGMs with materials based on metal oxide, nitrogen doped carbon, alloys, *etc.*, Pt and its alloys are still recognized as the most feasible materials to catalyse the oxygen reduction reaction (ORR) in the acidic environment of PEMFC cathodes.[8–14] Hence, a combination of optimization of the electrochemical activity and utilization of Pt has become one of the major tasks in the development of PEMFCs technologies. On one hand, core–shell structures and nanoframe structures have been intensively studied due to their advantages in terms of extending the surface area through their delicate nanostructure.[1] These studies are usually synergetic with the alloy effects to adjust the electron structure to achieve an optimized ORR activity. On the other hand, the catalyst layer with well-defined nanostructures that lead to effective electrochemical processes, namely the ordered electrode, is another route to achieve high utilization and activity of Pt.[15]

The ordered structured electrode, proposed by Middleman in 2002, in which electron, proton, reactant and product transport pathways were perpendicular to the membrane, was designed for maximizing the catalyst utilization and decreasing the mass transfer resistance of PEMFCs.[16] A significant method to construct the above electrode structures was proposed by 3M Co., and the as-prepared electrode was denoted as a nanostructured thin film (NSTF) catalyst.[5,17,18] Such ordered arrays were composed of organic crystal substrates and columnar PGM arrays growing along the substrates. This orderliness at the multi-scale could be regarded as an effective approach to enhance catalyst utilization and mass transport compared to those of traditional electrodes with randomly arranged catalyst particles and mass transport channels based on carbon materials. Nevertheless, the insulation of both electrons and ions of the organic substrates in an NSTF catalyst and their rigorous synthesis and transfer processes could be the potential drawbacks for their further application. Additionally, other substrate materials used for this ordered electrode have rarely been reported.

Recently, many researchers have employed conductive supports to form advanced electrode structures, such as carbon nanotubes (CNTs), carbon nanofibers (CNFs) or metal dioxides.[8,19–21] In our previous studies, conductive polymers, such as polypyrrole (PPy) and polyaniline (PANI), were developed as

[a]Division of Fuel Cells and Battery, Dalian National Laboratory for Clean Energy, Dalian Institute of Chemical Physics, Chinese Academy of Sciences, Dalian, China 116023. E-mail: gqsun@dicp.ac.cn; suliwang@dicp.ac.cn

[b]University of Chinese Academy of Sciences, Beijing, China 100049

† Electronic supplementary information (ESI) available: SEM and TEM images; XRD patterns; CO stripping, EIS, and PEMFC performance results. See DOI: 10.1039/c7ta02500a

membrane electrode assemblies (MEAs) in ordered nanostructures.[22–24] With facile preparation procedures, excellent physical and electrochemical properties were achieved for the construction of ordered mass transport pathways at the meso-scale. However, based on these substrates, the active sites with well-defined electrochemical surfaces have still been seldom studied to the best of our knowledge, which should be recognized as the core factor attributed to the performance of electrochemical devices.

In this study, we, for the first time, propose a hierarchically ordered electrode with crystallographically oriented Pt nanowhisker arrays anchored on vertically aligned PANI nanowires. By optimizing the fabrication conditions of chemical polymerization and magnetron sputtering, the structural parameters of this ordered electrode are controlled to meet the requirements of electrochemical reactions and mass transport at the micro- and meso-scales. Its performance in electrochemically catalysing the ORR and as the PEMFC cathode for the ordered electrode is also measured.

Experimental section

Preparation of PANI nanowires

The experimental details of preparing PANI nanowires could be found in our previous work.[22] In brief, an aniline monomer (0.186 g, AR, Tianjin Damao Reagent) and ammonium persulfate (0.304 g, APS, AR, Tianjin Damao Reagent) were added into a 200 mL $HClO_4$ solution (aqueous, 1 M). A piece of gas diffusion layer (GDL) (3×3 cm^2) was immersed in the mixed solution, where the MPL of the GDL faced the solution while the other side was sealed. Then, the mixture was kept still for 24 h. Finally, the GDL was taken out and washed with deionized water. The PANI nanowires polymerized at 270 K, 277 K and 295 K were denoted as PANI-GDL-1, PANI-GDL-2, and PANI-GDL-3.

Preparation of Pt–PANI-GDL ordered electrodes

Platinum was sputtered on the PANI-GDL-1, PANI-GDL-2, and PANI-GDL-3 by a physical vapour deposition (PVD, JCP-200) process to fabricate the Pt–PANI-GDL ordered electrodes, which were denoted as Pt–PANI-GDL-1, Pt–PANI-GDL-2 and Pt–PANI-GDL-3, respectively. For comparison, platinum was sputtered on the GDL to prepare the Pt–GDL electrode. All the above-mentioned deposition processes were performed for 300–320 s in an argon atmosphere with a working pressure of 0.35 Pa.

To study the formation mechanism of Pt on PANI nanowires, the deposition time was maintained at 1 min, 5 min and 10 min, while the substrate temperature was kept at 277 K and other conditions remained unchanged while fabricating the three samples.

Physical characterizations

The morphologies and properties of the Pt–PANI-GDL ordered electrodes and Pt–GDL electrode were investigated *via* a field emission scanning electron microscope (FESEM, JSM-7800F), transmission electron microscope (TEM, JEOL-2100), X-ray diffraction (XRD, RIGAKU Miniflex600) and X-ray photoelectron spectroscopy (XPS, ESCALAB 250Xi). The growth density of PANI nanowires could be calculated *via* a method described in the ESI.†

Fabrication of MEAs

To investigate the influence of the Pt–PANI-GDL ordered electrodes on the performance of PEMFCs, the MEAs with these electrodes were fabricated as follows. The Pt–PANI-GDL ordered electrodes (Pt–PANI-GDL-1, Pt–PANI-GDL-2, and Pt–PANI-GDL-3) with a Pt loading of 0.078–0.095 mg cm^{-2} were used as the cathodes. An anode was prepared by spraying catalyst ink composed of commercial 60 wt% Pt–C (Johnson Matthey Co.) and Nafion® ionomer on the GDL with a Pt loading of 0.101 mg cm^{-2}. The MEAs with an active area of 2×2 cm^2 were assembled through pressing the Nafion®212 membranes sandwiched between the cathode and the anode at 393 K with 200 kg cm^{-2} pressure for 1 min. For comparison, MEAs were prepared by employing the Pt–GDL electrode with a Pt loading of 0.105 mg cm^{-2}, and a commercial catalyst (0.120 mg cm^{-2}, Pt–C, 60 wt%, Johnson Matthey Co.) coated electrode as the cathodes with the same assembly method.

Electrochemical measurement and PEMFC single cell tests

A CHI 760B electrochemical workstation was used for the electrochemical measurements in a three-electrode electrochemical cell installed with a platinum wire as the counter electrode and a saturated calomel electrode (SCE) as the reference electrode. The Pt–PANI-GDL ordered electrodes, Pt–GDL electrode, and Pt–C (JM) electrode fixed by electrode holders were immersed in solutions as the working electrode. Cyclic voltammetry (CV) and oxygen reduction reaction (ORR) curves were obtained in N_2 or O_2 saturated $HClO_4$ electrolyte with a scan rate of 20 mV s^{-1} in the range of 0.05–1.2 V *vs.* the reversible hydrogen electrode (RHE). CO stripping measurement was conducted in a CO saturated $HClO_4$ electrolyte (0.1 M) at 0.1 V *vs.* the RHE kept for 20 min, and then in a N_2 saturated $HClO_4$ electrolyte (0.1 M) with the same potential kept for 60 min, and thus cyclic voltammetry (CV) at a scan rate of 20 mV s^{-1} was performed. The electrochemical surface areas (ECSAs) could be calculated by integrating the CO stripping peak.[25]

The single cell performance was evaluated using a fuel cell test system (G20, Greenlight Innovation and ELOAD, Arbin Instruments) at 343 K. The anode side was fed with hydrogen at a flow rate of 50 mL min^{-1} and the cathode side was fed with oxygen at a flow rate of 150 mL min^{-1} without backpressure. The hydrogen and oxygen were both externally humidified at a dew point temperature of 343 K. The oxygen gain of PEMFCs was the difference of cell voltages at the same current density when the cathode was fed with oxygen or air (without backpressure). Electrochemical impedance spectroscopy (EIS) was conducted at 343 K on an electrochemical workstation (SI1287, SI1260, Solartron Co.) with humidified oxygen at a flow rate of 150 mL min^{-1} and the anode was fed with humidified hydrogen at a flow rate of 50 mL min^{-1}. The alternating current (AC) potential frequency range was 10 kHz to 0.1 Hz with an amplitude of 10 mV.

Results and discussion

The construction processes of the hierarchical nanostructure are illustrated in Scheme 1, with the comparison of those of the traditional sputtering electrode. Apparently, with the aid of the nanowires introduced *via* the chemical deposition of PANI, the growth behaviour of Pt crystals could be remarkably changed compared to that of the traditional one. Normally, the Pt layer sputtered on the carbon powder substrate appears as disordered clusters assembled by the polycrystalline particles, as illustrated in Fig. S1.† However, with the fabrication of the ordered PANI nanowires, the sputtered Pt layers exhibit a more delicately secondary structure based on the PANI substrate, as shown in Fig. 1. In a typical PANI sample with a fabrication temperature of 277 K (Fig. 1a and b), the uniform nanowires possess an average diameter of 61 nm, an average length of 194 nm, and a growth density of 78 μm^{-2}, which are similar to those of our previous studies.[22] We have further prepared three PANI samples with different average lengths ranging from 140 to 302 nm by simply adjusting the polymerization temperature, as shown in Fig. S2.† After the sputtering process of Pt, the uniform arrays of nanoclusters growing on PANI nanowires could be recognized, as shown in Fig. 1c and d. As a result, the Pt coated PANI nanowires demonstrate an expanded average diameter of 80 nm and a length of 219 nm.

To further investigate the morphological and structural details of the Pt layers, HRTEM tests were conducted on the Pt–PANI-GDL sample, as shown in Fig. 2. Noticeably, the average thickness of the deposited Pt layer is about 8.9 nm, as measured in Fig. 2b, which is consistent with the expansion of the above-mentioned nanowire diameter, and also in accordance with the XRD results with a Pt particle size of 8.2 nm (Fig. S4†). Remarkably, we can also find evidence of the unique growth of Pt crystalline nanowhiskers based on the polymer substrate, as illustrated in Fig. 2c. Along the axial direction of the PANI nanowires, the Pt nanowhisker arrays are densely arranged according to their orderliness, with an approximate growth angle of 67°, as measured in Fig. 2c. Additionally, the Pt nanowhiskers shown in the high resolution image (Fig. 2d) indicate a truncated pyramid-like shape for the tip parts, with an angle of 67° between the two side edges. These microstructures of the Pt nanowhiskers might be well consistent with the face-centred cubic structure of the Pt crystal.[26] According to the above result, the mechanism of Pt nanowhiskers was proposed as illustrated in Fig. 2e, namely, the initially sputtered Pt atoms could be strongly bonded with the polymer substrate to form microislands. With the growing amount of the sputtered metal, the octahedral nature of the Pt crystals leads to the formation of pyramid like nanoislands. With the strong chemical bonds between the metal and the substrate, the growth of the Pt crystallites would occur along the direction with lower Miller index planes for maintaining a smaller surface free energy.[18] Hence, because the (111) facets possess the lowest surface free energy, the crystalline structure of the sputtered Pt nanowhiskers would expose such predominated planes, and follow the growth direction as illustrated. The crystallographic details could also be confirmed by the diffraction patterns obtained from Fourier transformation, as shown in the inset image of Fig. 2d. Such a growth mechanism could also be proved by the morphological images at different sputtering stages of Pt, as shown in Fig. S3.† At the initial stage with a relatively short sputtering time, the Pt layer consists of small particles (Fig. S3a†), while with the sputtering time increasing, the Pt nanowhiskers are formed (Fig. S3b and c†).

The interactions between the Pt and the PANI substrate were intensively studied with the XPS tests, as shown in Fig. 3. Compared to the sample with Pt sputtered on traditional carbon

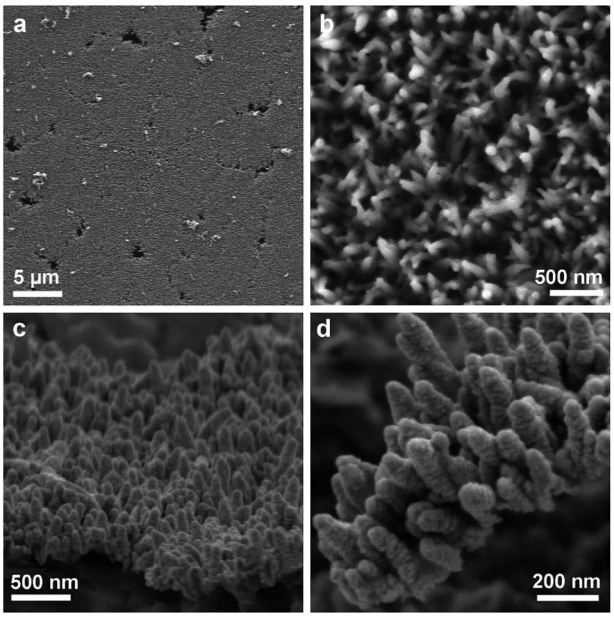

Fig. 1 SEM images of PANI nanowires and the Pt–PANI-GDL ordered electrode; (a and b) top views of vertically aligned PANI nanowires (PANI nanowires were polymerized at 277 K) with different magnifications; (c and d) side views of Pt nanowhiskers being deposited on PANI nanowires with different magnifications.

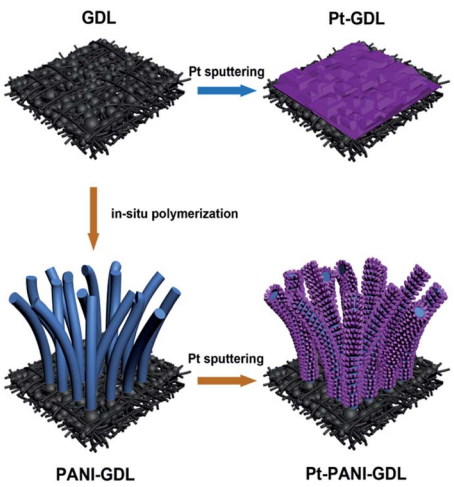

Scheme 1 Schematics of the fabrication process of the Pt–PANI-GDL ordered electrode and Pt–GDL electrode.

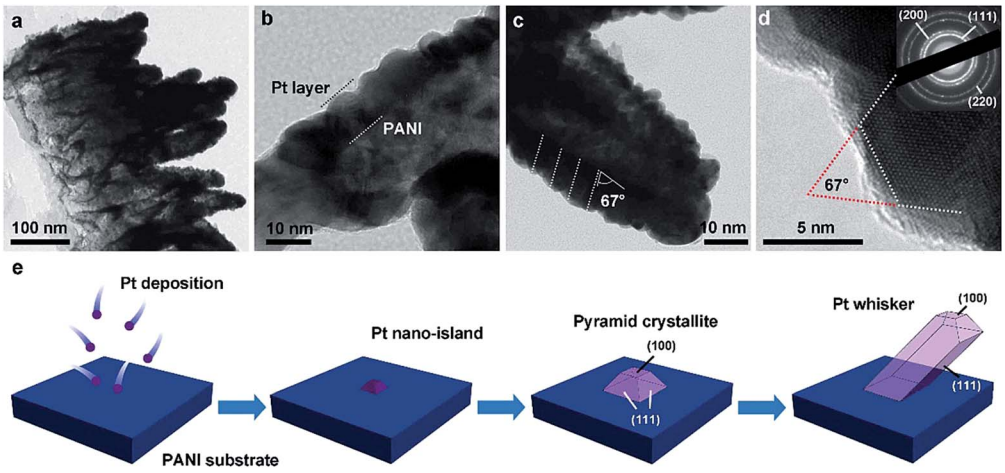

Fig. 2 TEM images of the Pt–PANI-GDL ordered electrode with different magnifications (a–d) and the schematics of the growth process of Pt nanowhiskers (e). The mechanism of Pt nanowhisker formation: at the initial stage with a relatively short sputtering time, the Pt layer consists of small particles, while with the sputtering time increasing, the Pt nanowhiskers are formed.

materials (GDL), the spectroscopic peak attributed to the Pt 4f orbital located on PANI nanowires could be observed with a positive shift of 0.1 eV, indicating partial transfer of the outer-layer electrons.[27] To further analyse the electron structures of N 1s in the PANI substrate as shown in Fig. 3b, three peaks are obtained by the deconvolution of the N 1s core level spectra correlating to the three electron states of =–N– (398 eV), –N= (399 eV), and $-N^{+}$ (401 eV).[28] Obviously, the Pt–PANI-GDL could be observed with a negative shift and increased percentage of =N–, compared with that of PANI-GDL, indicating that there exists electron transfer between the nitrogen containing groups and Pt atoms. Therefore, these phenomena demonstrate the interactions between the PANI substrate and the metal whiskers.[28,29]

With the unique crystallographic structures and chemical interactions towards the polymer substrates, the Pt nanowhisker arrays grown on the ordered PANI nanowires could demonstrate outstanding properties in their electrochemistry. We conduct serial experiments directly on the electrode samples in the three-electrode system to evaluate the electrochemical catalytic performance for the ORR. Attributed to the electrochemical redox and capacitance properties of PANI, the CV curve of the Pt–PANI-GDL sample is dramatically different from that of the Pt–GDL and Pt–C (JM) samples, for the hydrogen desorption peaks largely covered by PANI signals, as shown in Fig. 4a. However, the electrochemical surface area (ECSA) could be obtained by the method of CO stripping, as shown in Fig. S5,† which is found to be 11–14 $m^2\ g_{Pt}^{-1}$ for the Pt–PANI-GDL samples and 12 $m^2\ g_{Pt}^{-1}$ for the Pt–GDL sample. Despite the similarity of the ECSA for different samples, the polarization curves exhibit noticeable enhancement of the ORR activity for the hierarchically structured sample. As illustrated in Fig. 4b, the onset potential and the half-wave potential of the ORR polarization curve for the Pt–PANI-GDL sample are much more positive compared to that of the Pt–GDL sample, while a positive shift of 11 mV is observed for the half-wave potential of the ordered electrode. Ascribed to the mass loadings and ECSAs of Pt, the mass activity (MA) and specific activity (SA) at 0.9 V (*vs.* the RHE) of the Pt–PANI-GDL sample are found to be 14.7 mA mg_{Pt}^{-1} and 0.108 mA cm^{-2}, respectively, which demonstrate 32% and 15% enhancement compared to those of the Pt–GDL sample. Additionally, the MA of the Pt–PANI-GDL is also comparable with that of the commercial catalyst sample (Pt–C JM), while the SA of the ordered electrode is 2.19-fold greater than that of the commercial one. This enhancement in the electrochemical catalytic activity would be derived from two crucial aspects. The first reason should be the interactions between the metal and the substrate for adjusting the electron structure of Pt, as evidenced in the XPS results. The partially transfer of the outer-layer electrons of Pt could slightly weaken the adsorption of the intermediate OH species, which has been proved to boost the ORR activity and durability.[30,31] On the other hand, the preferential crystallographic orientation in the growth of Pt nanowhiskers exposes the electrochemically active facets of Pt (111) with a higher surface-area ratio, as illustrated in Fig. 2.[17,32] These combinational factors could enable the ordered electrode to gain an enhanced activity towards the ORR.

To further investigate the performance in the applied situation of PEMFCs, the Pt–PANI-GDL, the Pt–GDL, and the Pt–C (JM) samples are assembled as the cathodes and tested, and the results are provided in Fig. 5. As the enhancement in the half-

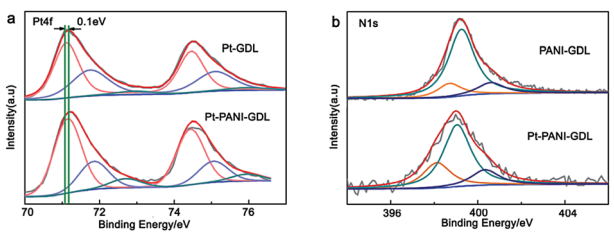

Fig. 3 XPS spectra of the Pt 4f peaks of the Pt–GDL electrode and Pt–PANI-GDL electrode (a), and N 1s peaks of the PANI-GDL electrode and Pt–PANI-GDL electrode (b).

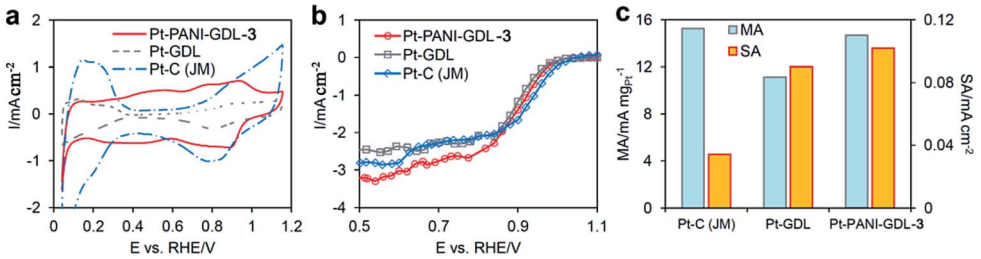

Fig. 4 Electrochemical measurements of the Pt–GDL electrode and Pt–PANI-GDL ordered electrode. (a) CV curves measured using different electrodes at a 20 mV s^{-1} scan rate in 0.1 M $HClO_4$ saturated by N_2; (b) ORR curves measured at a 20 mV s^{-1} scan rate in 0.1 M $HClO_4$ saturated by O_2 using the Pt–GDL electrode and Pt–PANI-GDL ordered electrode which are fixed by electrode holders; (c) mass activity (MA) and specific activity (SA) at 0.9 V *vs.* the RHE.

cell measurement, the single cell equipped with the ordered electrode also remarkably outperforms that of the Pt–GDL sample with an increase of 90% in the peak power density of the polarization curve, and also surpasses the Pt–C (JM) sample with an enhancement of 39% in the cathode mass specific power density. The improvement in the electrochemical catalysis could be further evidenced in the electrochemical impedance spectra (EIS) results, as shown in Fig. S6.† Obviously, the diameter of the first semicircle in the spectral curve in the high frequency region for the ordered electrode sample, which represents the resistance of electron transfer of the electrochemical processes, is much smaller than that for the Pt–GDL sample both under low current density (100 mA cm^{-2}) and high current density (500 mA cm^{-2}) conditions. It is also noticed that the reinforcement is attributed not only to the strengthened electrochemical activity in the low current density region, but also to the observed improvement in the mass transport dominated region, especially compared to the commercial Pt–C sample with randomly distributed structures. The Pt–PANI-GDL electrode would benefit from the ordered structure of the PANI nanoarrays to enhance the mass transport in the electrochemical processes, as our previous studies discussed. To intensively investigate the effect of mass transport, the Pt–PANI-GDL samples with different orderliness are assembled as MEAs, and tested as well (Fig. S7†). As expected, the higher ordered sample outperforms the ones that possess lower orderliness in their structure when the polarization curves are normalized to the Pt loadings. The tests of oxygen gain, which show voltage differences between the cathode inlet conditions of oxygen and air, could directly indicate the mass transport properties of different electrode samples, as shown in Fig. S6.†

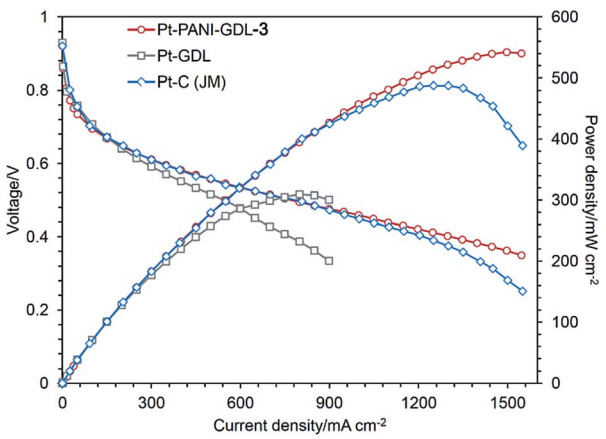

Fig. 5 PEMFC polarization curves and power density curves of the Pt–PANI-GDL-3 ordered electrode and Pt–GDL electrode. The cell temperature is 343 K; the flow rates of hydrogen and oxygen are 50 mL min^{-1} and 150 mL min^{-1} without backpressure.

Conclusions

Here in this work, we design and fabricate a hierarchically ordered electrode with crystallographically oriented Pt nanowhisker arrays grown on the surface of PANI nanowires. By adopting the substrate of PANI, the nitrogen containing groups could anchor the Pt atoms during the sputtering process, and help to realize the preferential growth of the truncated pyramid-like Pt nanowhiskers. The electron modification effects of the substrate, in association with the enhanced exposure of Pt (111) facets, greatly boost the electrochemical activity towards the ORR with a 2.19-fold enhancement of the specific activity and a similar mass specific activity at 0.9 V (*vs.* the RHE), compared to the state-of-the-art Pt–C electrode. Additionally, with the aid of the improved mass transport within the array structure, this well-tailored electrode achieves a more significant success when applied as the cathode of a PEMFC with a cathode mass specific power density of 5.7 W mg_{Pt}^{-1} and a 39% increase compared to that of a traditional one. Hence, this work proposes a promising approach to construct a well defined electrode architecture with ideal micro- and meso-structures for the electrochemical processes of charge transfer and mass transport. Such demonstrated electrode structures not only could have the potential to be the substitute for traditional disordered electrodes, but also would enable the development of a large range of electrochemical energy conversion devices.

Acknowledgements

This work is financially supported by the National Natural Science Foundation of China (No. 21503228 and No. 21506209).

References

1 S. Sui, X. Wang, X. Zhou, Y. Su, S. Riffat and C. j. Liu, *J. Mater. Chem. A*, 2017, **5**, 1808–1825.
2 M. K. Debe, *Nature*, 2012, **486**, 43–51.
3 S. Litster and G. McLean, *J. Power Sources*, 2004, **130**, 61–76.
4 J. H. Wee, K. Y. Lee and S. H. Kim, *J. Power Sources*, 2007, **165**, 667–677.
5 D. A. Cullen, M. Lopez-Haro, P. B. Guillemaud, L. Guetaz, M. K. Debe and A. J. Steinbach, *J. Mater. Chem. A*, 2015, **3**, 11660–11667.
6 A. Brouzgou, S. Q. Song and P. Tsiakaras, *Appl. Catal., B*, 2012, **127**, 371–388.
7 A. Morozan, B. Jousselme and S. Palacin, *Energy Environ. Sci.*, 2011, **4**, 1238–1257.
8 J. Y. Cheon, C. Ahn, D. J. You, C. Pak, S. H. Hur, J. Kim and S. H. Joo, *J. Mater. Chem. A*, 2013, **1**, 1270–1283.
9 S. Yu, R. Liu, W. Yang, K. Han, Z. Wang and H. Zhu, *J. Mater. Chem. A*, 2014, **2**, 5371–5378.
10 M. N. Banis, S. Sun, X. Meng, Y. Zhang, Z. Wang, R. Li, M. Cai, T.-K. Sham and X. Sun, *J. Phys. Chem. C*, 2013, **117**, 15457–15467.
11 Q. Du, J. Wu and H. Yang, *ACS Catal.*, 2014, **4**, 144–151.
12 Y. Zhou, K. Neyerlin, T. S. Olson, S. Pylypenko, J. Bult, H. N. Dinh, T. Gennett, Z. Shao and R. O'Hayre, *Energy Environ. Sci.*, 2010, **3**, 1437–1446.
13 J. Wang, B. Li, T. Yersak, D. Yang, Q. Xiao, J. Zhang and C. Zhang, *J. Mater. Chem. A*, 2016, **4**, 11559–11581.
14 S. M. Alia, K. Jensen, C. Contreras, F. Garzon, B. Pivovar and Y. Yan, *ACS Catal.*, 2013, **3**, 358–362.
15 A. Bonnefont, P. Ruvinskiy, M. Rouhet, A. Orfanidi, S. Neophytides and E. Savinova, *Wiley Interdiscip. Rev.: Energy Environ.*, 2014, **3**, 505–521.
16 B. E. Middelman, *Fuel Cells Bull.*, 2002, **2002**, 9–12.
17 C. D. F. Vandervliet, C. Wang, D. Tripkovic, D. Strmcnik, X. F. Zhang, R. T. Atanasoski, M. K. Debe, N. M. Markovic and V. R. Stamenkovic, *Nat. Mater.*, 2012, **11**, 1051–1058.
18 M. K. Debe, *J. Electrochem. Soc.*, 2013, **160**, 522–534.
19 Z. Tang, H. Y. Ng, J. Lin, A. T. S. Wee and D. H. C. Chua, *J. Electrochem. Soc.*, 2010, **157**, B245–B250.
20 M. Li, Y. Xiong, X. Liu, C. Han, Y. Zhang, X. Bo and L. Guo, *J. Mater. Chem. A*, 2015, **3**, 9658–9667.
21 C. Marichy, G. Ercolano, G. Caputo, M. G. Willinger, D. Jones, J. Rozière, N. Pinna and S. Cavaliere, *J. Mater. Chem. A*, 2016, **4**, 969–975.
22 X. Fu, S. Wang, Z. Xia, Y. Li, L. Jiang and G. Sun, *Int. J. Hydrogen Energy*, 2016, **41**, 3655–3663.
23 Z. Xia, S. Wang, L. Jiang, H. Sun and G. Sun, *J. Power Sources*, 2014, **256**, 125–132.
24 Z. Xia, S. Wang, Y. Li, L. Jiang, H. Sun, S. Zhu, D. S. Su and G. Sun, *J. Mater. Chem. A*, 2013, **1**, 491–494.
25 S. Wang, T. Cochell and A. Manthiram, *Phys. Chem. Chem. Phys.*, 2012, **14**, 13910–13913.
26 T. K. L. Gancs, M. K. Debe, R. Atanasoski and A. Wieckowski, *Chem. Mater.*, 2008, **20**, 2444–2454.
27 H. I. Lee, S. H. Joo, J. H. Kim, D. J. You, J. M. Kim, J. N. Park, H. Chang and C. Pak, *J. Mater. Chem.*, 2009, **19**, 5934–5939.
28 D. He, C. Zeng, C. Xu, N. Cheng, H. Li, S. Mu and M. Pan, *Langmuir*, 2011, **27**, 5582–5588.
29 D. Yan, S. Dou, L. Tao, Z. Liu, Z. Liu, J. Huo and S. Wang, *J. Mater. Chem. A*, 2016, **4**, 13726–13730.
30 Z. Xia, S. Wang, L. Jiang, H. Sun, S. Liu, X. Fu, B. Zhang, D. Sheng Su, J. Wang and G. Sun, *Sci. Rep.*, 2015, **5**, 16100–16110.
31 J. Greeley, I. E. Stephens, A. S. Bondarenko, T. P. Johansson, H. A. Hansen, T. F. Jaramillo, J. Rossmeisl, I. Chorkendorff and J. K. Norskov, *Nat. Chem.*, 2009, **1**, 552–556.
32 M. Shao, Q. Chang, J. P. Dodelet and R. Chenitz, *Chem. Rev.*, 2016, **116**, 3594–3657.